SCA-9726

PREDICTION OF ELECTRICAL AND FLOW PROPERTIES OF RESERVOIR ROCKS OF VARYING WETTABILITY CHARACTERISTICS

J.L. Wang and A. Gupta, School of Petroleum & Geol. Eng., Univ. of Oklahoma, Norman, OK 73019
R.N. Vaidya, J.R. Bulau and M.M.Honarpour,Mobil Technology Center, Dallas, TX 75244

Abstract

A model for predicting the resistivity and relative permeability behavior of reservoir rocks samples is presented, in which the porous media is represented as a network of pore bodies and pore throats. Pore throats are modeled as tubes of triangular cross-section such that the contribution of corners and thin films to the electrical and fluid transport is conveniently included, in addition to the primary network transport. Mathematical formulations for the electrical and fluid transport in individual tubes containing one and two fluid phases are incorporated in the model. Pore size distribution functions interpreted from mercury injection capillary pressure curves are used and the effect of intrinsic wettability of the sample on the electrical resistivity and relative permeability to wetting and non-wetting fluids is studied by varying the film thickness according to the measured disjoining pressure isotherm. Sensitivity analysis indicates that model predictions are very sensitive to the coordination number, the shape factor and the parameters relating pore length to its cross-section area. According to the model predictions, wettability plays a critical role in determining the electrical and fluid transport in reservoir rocks and the apparent wettability of sample may be different from the intrinsic wettability. Model predictions are in reasonable agreement with the measured resistivity index vs. saturation data.

Introduction

Experimental determination of resistivity and relative permeability behavior of reservoir rock is prohibitively expensive and subject to uncertainties related to the alteration of wettability and pore structure of samples during coring and transport to the surface. Much research effort has been devoted in the past to model electrical and transport properties, including percolation and Effective Medium Theory (EMT)[1-3]. The effect of wettability, that manifests as corner flow and film flow, has rarely been included in the reported models. Further, most models treat pore-throats as cylindrical tubes.

In this study, the reservoir rock is represented as a network of pore bodies and pore throats arranged in a lattice in which the pore bodies are modeled as spheres and pore throats as triangular tubes. Water-wet, mixed-wet and oil-wet reservoirs are considered in the model simulations. The motivation for using a triangle as pore throat shape becomes apparent on inspection of thin sections of samples representing sandstone reservoirs, which reveal that the pore cross-section is very close to triangular shape[4], as shown in Fig.1. Similar observation were applicable to the thin sections for the sandstone

samples studied in this work. Further, triangular cross-section facilitates modeling of corner flow and allows means for studying the effect of pore shape.

Model Development and Formulation

The development of a model for the prediction of resistivity index and relative permeabilities of reservoirs of varying wettability characteristics were presented by Wang[5]. The formulation and model implementation is based on the assumptions that: (1) the wetting and non-wetting fluids can co-exist and flow in the same channel such that the wetting phase occupies corners and forms a continuous thin film on the flat walls of the triangular channels penetrated by the non-wetting phase; (2) all fluids are Newtonian and in laminar flow; (3) no slip occurs at the water and oil interface; (4) fluids and rock-matrix are incompressible.

The connectivity of the model network, as shown in Fig.2, is defined by a coordination number, Z, which is the number of pore throats connected to each pore body. A representative pore segment in the network consists of one pore throat and the 2/Z fraction of a pore body, as shown in Fig.3. The electrical and hydraulic conductance of network are determined based on the distribution of conductance for pore segments in the network. EMT is used to determine the representative conductance for a network that is equivalent to the network of pore segments with specified conductance distribution.

The volume of a pore segment (V_p) is calculated with the knowledge of its cross-sectional area and length, expressed in terms of representative parameters such that,

$$V_p = \left(\frac{C}{4G} r_i^{\alpha-1} + \frac{8\pi}{3Z} a_r^3\right) r_i^3 \qquad (1)$$

where r_i is the incircle radius of triangle, a_r is the aspect ratio defined as the ratio of the pore body radius to the pore throat incircle radius, C and α are constants that relate the length of a pore throat to its incircle radius. A shape factor, G, is defined as the ratio of the cross-sectional area (S) to the square of the perimeter of the triangle (P)[6] . Shape factor ranges from nearly zero for a slit-shaped triangle to a maximum value of 0.04811 for an equilateral triangle.

After the drainage of wetting fluid from the central region of a pore segment, when its threshold capillary pressure is exceeded, the wetting phase is retained in the corners and the thin film coating the walls of the triangular tube, as indicated in Fig. 4. At a capillary pressure higher than the threshold value, the corner radius r is less than r_d, the corner radius at drainage capillary pressure, and the wetting phase is drained from the corners and the thin film region. The total volume of the wetting phase in a pore segment after it has been drained by the non-wetting phase is

$$V_{cf} = \left[\frac{C(1-4\pi G)}{4G} r^2 + h\left(\frac{r_i - r}{2G} C + \frac{8}{Z}\pi a_r^2 r_i^{2-\alpha}\right)\right] r_i^{\alpha} \qquad (2)$$

For a planar thin film, the thickness is governed by capillary pressure according to the disjoining pressure isotherm. For many oil-water systems, the exponential relationship between capillary pressure and film thickness[7] is satisfactory,

$$h = -l_o \cdot Ln\left(P_c / A_k\right), \quad (P_c < A_k) \tag{3}$$

where P_c is the capillary pressure and, A_k and l_o are constants that depend on the chemistry of the mineral/wetting and wetting/non-wetting interfaces.

Before the drainage of a water-wet pore segment, it is occupied by water and the path for electrical conduction consists of a pore throat in series with fractions of two adjacent pore bodies. If ρ is the resistivity of brine, the resulting electrical conductance of a pore segment occupied by water is[5]

$$g = 1/\left[\rho\left(4GCr_i^{\alpha-2} + \left(1/Za_r r_i\right)\right)\right], \tag{4}$$

During the drainage of pore segments in a water-wet rock by oil, the water is assumed to be retained in the corners and as thin film, as illustrated in Fig.4, providing the electrical conductance. The electrical conductance of a drained pore segment is[5]

$$g_{cf} = \frac{1}{\rho\left[\dfrac{4GCr_i^{\alpha}}{(1-4\pi G)r^2 + 2(r_i - r)h} + \dfrac{1}{Zh}\right]} \tag{5}$$

In order to calculate the relative permeability values, relationships for hydraulic conductance to water and oil through individual pore segments are required. For pore segments occupied by one fluid, hydraulic conductance of a pore throat is[5]

$$g_{wt,S_w=1} = \frac{r_i^4}{32G\mu_w L_t}, \tag{6}$$

and, the hydraulic conductance of a pore body is[5]

$$g_{wb,S_w=1} = \frac{\pi}{8\mu_w\left[\dfrac{\sqrt{r_b^2 - r_i^2}}{r_b^2 r_i^2} + \dfrac{1}{2r_b^3}\ln\left(\dfrac{r_b + \sqrt{r_b^2 - r_i^2}}{r_b - \sqrt{r_b^2 - r_i^2}}\right)\right]} \tag{7}$$

where r_b is the pore body radius which is related to the pore throat incircle radius through the aspect ratio.

At a stage of drainage characterized by a capillary pressure and a corner radius r_d (the corresponding incircle radius being r_{id}), smaller pores are totally occupied by water. For larger pore throats occupied by oil with water present in corners and film, the hydraulic conductance to water is[5] given by Eq.8, in which $\alpha = (\pi - D)/2$, $\beta = (\pi - E)/2$, and $\gamma = (\pi - F)/2$; D, E and F are the vertex angles of a triangular tube as illustrated in Fig.4;

$$g_{wtcf,S_w} = \frac{2h}{\mu_w}\left\{\begin{array}{l} a_1(\alpha+\beta+\gamma) + b_1 Ln\left[(\tan\alpha+\sec\alpha)(\tan\beta+\sec\beta)(\tan\gamma+\sec\gamma)\right] \\ + c_1(\tan\alpha+\tan\beta+\tan\gamma) + \dfrac{h}{12}\left(r_{id} + \dfrac{A_{nw}}{P_{nw}}\right)\left(P_{nw} - 2\pi r_d\right) \end{array}\right\}\frac{1}{L_t} \tag{8}$$

a_1, b_1, c_1 are constants at a specified fluid saturation, such that

$$a_1 = -\left[\frac{\left(3A_{nw}/P_{nw}\right)+\left(5r_{id}/2\right)}{24}\right]r_d^2 \; ; \; b_1 = \left[\frac{\left(A_{nw}/P_{nw}\right)+\left(r_{id}/2\right)}{12}\right]\left(1+\frac{h}{r_d}\right)r_d^2$$

$$c_1 = \left[\frac{\left(A_{nw}/P_{nw}\right)+\left(3r_{id}/2\right)}{24}\right]\left(1+\frac{h}{r_d}\right)^2 r_d^2 .$$

where A_{nw} and P_{nw} are the cross-sectional area and the perimeter of the oil phase, respectively. The equation for the hydraulic conductance to water through the thin film in a pore body is derived as[5]:

$$g_{wbf,S_w} = \frac{\pi h^2\left(r_{id} + A_{nw}/P_{nw}\right)}{6\mu_w \ln\left(a_r + \sqrt{a_r^2 - 1}\right)} \tag{9}$$

The hydraulic conductance to oil through a pore throat is[5]

$$g_{otSw} = A_{nw}\left[\frac{\left(r_{id}-h\right)^2}{8\mu_o} + \frac{h}{2\mu_w}\left(\frac{A_{nw}}{P_{nw}} + \frac{r_{id}}{2}\right)\right]\frac{1}{L_t} , \tag{10}$$

and the hydraulic conductance to oil through a pore body is[5]

$$g_{ob,S_w} = \frac{\pi}{8\mu_o\left[\frac{\sqrt{\left(r_b-h\right)^2 - r_{id}^2}}{\left(r_b-h\right)^2 r_{id}^2} + \frac{1}{2\left(r_b-h\right)^3}\ln\frac{\left(r_b-h\right)+\sqrt{\left(r_b-h\right)^2 - r_{id}^2}}{\left(r_b-h\right)-\sqrt{\left(r_b-h\right)^2 - r_{id}^2}}\right]} \tag{11}$$

The hydraulic conductances to water and oil under varying saturation states are obtained by adding pressure drops through each component since a pore segment can be treated as being composed of conductors in series,

$$\frac{1}{g_{i,S_w}} = \frac{2}{Z}\frac{1}{g_{ib,S_w}} + \frac{1}{g_{it,S_w}}, \qquad i = w, o. \tag{12}$$

Simulation of Drainage Process in the Network

At a stage of drainage, characterized by a drainage radius r_d, and pore throat incircle radius r_{id}, the fraction of pores allowed to be occupied by the non-wetting phase is

$$X_{nw} = \int_{r_{id}}^{\infty} f(r_i)dr_i \tag{13}$$

However, only the pores with incircle radius greater than r_{id} and accessible to the continuous phase may be occupied by the non-wetting fluid. The fraction of the pores accessible to the non-wetting fluid is denoted as X_a and is a function of the allowable fraction, X_{nw}, as illustrated in Fig.5. The accessibility function for Bethe trees, presented by Fisher and Essam[8], as implemented by Larson[9], and Larson and Morrow[10], is utilized for obtaining the results presented. Using a value of 170 as the characteristic

number of pore segments, N, provides an accessibility function nearly identical to that for infinitely large network.

Effective Electrical Conductance of Network

Water is assumed to be the only fluid contributing to the electrical conductance. The microscopic conductances of individual pore-segments are replaced by a mean conductance value, such that the potential field produced by the random conductances is the same as that produced when all pore-segments have the mean value, represented by g_m. EMT[1,11,12] is utilized for this purpose. If the electrical conductance of an individual pore segment is g; the local deviations from the mean value, $(g\text{-}g_m)$, must add to zero over the network. This basis allows the calculation of the effective electrical conductance of the network, g_m,

$$\int_0^\infty \frac{g-g_m}{g+\left(\frac{Z}{2}-1\right)g_m} G(g)dg = 0 \ , \tag{14}$$

where $G(g)$ is conductance distribution, $G(g)dg$ is the probability of a pore segment having conductance between g and $g+dg$ and is related to the pore size distribution by

$$G\left(g(r_i)\right) = f(r_i)\left(\frac{dr_i}{dg(r_i)}\right) \tag{15}$$

Water saturation corresponding to g_m is

$$S_w = 1-\left(\frac{X_a}{X_{nw}}\right)\left[\int_{r_{id}}^\infty f(r_i)dr_i - \int_{r_{id}}^\infty \left(V_{cf}/V_p\right)f(r_i)dr_i\right] \tag{16}$$

The second part of the integral in Eq.16 represents the volume fraction occupied by water in the oil-penetrated pores.

Effective Hydraulic Conductance of Network to Oil and Water

Hydraulic conductance of the network to oil and water allows the determination of the relative permeability of network to oil and water, respectively. The effective hydraulic conductance to water at a specific S_w is obtained as a root of [5]

$$\begin{aligned}&\int_0^\infty \frac{g(r_i)-g_{mw,Sw}}{g(r_i)+\left(\frac{Z}{2}-1\right)g_{mw,Sw}} f(r_i)dr_i - \frac{X_a}{X_{nw}}\int_{r_{id}}^\infty \frac{g(r_i)-g_{mw,Sw}}{g(r_i)+\left(\frac{Z}{2}-1\right)g_{mw,Sw}} f(r_i)dr_i \\ &+\frac{X_a}{X_{nw}}\int_{r_{id}}^\infty \frac{g_{cf}(r_i)-g_{mw,Sw}}{g_{cf}(r_i)+\left(\frac{Z}{2}-1\right)g_{mw,Sw}} f(r_i)dr_i = 0\end{aligned} \tag{17}$$

and the effective hydraulic conductance to oil is obtained as a root of[5]

$$\frac{X_a}{X_{nw}}\int_{r_{id}}^{\infty}\frac{g(r_i)-g_{mo,Sw}}{g(r_i)+\left(\frac{Z}{2}-1\right)g_{mo,Sw}}f(r_i)dr_i=\frac{1-X_a}{\frac{Z}{2}-1} \tag{18}$$

It is assumed that the presence of water in thin film and corners allows the drainage process to be carried on until the oil phase penetrates the smallest available pore segment.

The relative permeability to water and oil are obtained from the respective effective hydraulic conductance

$$k_{rw}=\frac{K_w}{K}=\frac{g_{w,S_w}}{g_{w,S_w=1}}, \tag{19}$$

$$\text{and, } k_{ro}=\frac{K_o}{K}=\frac{g_{o,S_w}}{g_{w,S_w=1}}\frac{\mu_o}{\mu_w} \tag{20}$$

Determination of Model Parameters

Practical application of the model presented in this paper requires a determination of key parameters. Pore size distribution is obtained from mercury injection capillary pressure curve for the core samples by utilizing the methodology presented by Mishra and Sharma[13]. The characteristic number of pore segments, utilized in the percolation calculations, is 170. Fig.6(a) shows the volume fraction of pores of various sizes and Fig. 6(b) shows the pore size frequency distributions for an unconsolidated sample. The shape factor (G) is estimated from the thin section images for the sample. Several of the representative triangles were selected from which two angles are measured and then the shape factor is calculated using[5]

$$G=\frac{\sin D\sin E\sin(\pi-D-E)}{2\left[\sin D+\sin E+\sin(\pi-D-E)\right]^2} \tag{21}$$

The average value of the shape factor for S-28 is estimated to be 0.04526. Aspect ratio (a_r), coordination number (Z) and constants in the relationship between L_t and r_i (C and α) are estimated by measurements on several representative pore throat-body pairs selected from given thin section. The average aspect ratio for Sample S-28 is determined as 8.6. The number of pore throats surrounding the pore body are counted, although it was observed that estimation of three dimensional coordination number based on thin sections is not reliable. The coordination number for S-28 is estimated in the range of 6 to 15. Alternately, from percolation theory[8]

$$Z=\frac{1}{X_c}+1 \quad \text{(for Bethe trees)} \tag{22}$$

where X_c corresponds to the percolation threshold, and can be determined from mercury capillary pressure curve. For S-28, X_c is 0.05, and the coordination number is 21. C and α are determined by measuring the length and incircle radius of selected pore throats. C value is estimated in the range of 0.084 to 100, and the corresponding range for α is 2 to -0.204. Constants in the expression for film thickness, A_k and l_o, are obtained by fitting the

measured disjoining pressure isotherms[14] to be 5.73 x 10^4 pascals and 11.1 Angstroms, respectively.

Sensitivity Analysis and Optimization of Model Parameters

Sensitivity analysis is performed by varying one parameter and keeping other parameters constant. The effect of Z, G, h, C and α on resistivity index curve for Sample S-28 is illustrated in Figs.7 through 10. Resistivity index curve is highly sensitive to coordination number, to shape factor, to film thickness at low S_w, and to C and α. As Z, G , and h increase, resistivity index decreases. Resistivity index curve exhibits low sensitivity to film thickness at high S_w, and to the aspect ratio.

The effect of Z, G, C and α on relative permeability curves for Sample S-28 is shown as Figs.11 through 13. Relative permeability curves are highly sensitive to Z, C, and α-as Z increases, k_{rw} decreases and k_{ro} increases. Shape factor has negligible effect on k_{rw} but significant influence on k_{ro} - as G increases, k_{ro} increases. Aspect ratio and film thickness have negligible effect on relative permeability curves.

In order to match the experimental data and narrow the uncertainty, the model parameters are optimized using the solver utility in a MS-Excel spreadsheet, by matching the measured porosity, permeability and formation factor. The equations that relate formation factor, porosity and permeability to the model parameters are derived as:

$$F = 2\left(\sqrt{a_r^2 - 1} + Cr_{im}^{\alpha-1}\right)\left(4GCr_{im}^{\alpha-1} + \frac{1}{Za_r}\right) \tag{23}$$

$$\phi = \frac{\left(\frac{Z}{2}\right)\cdot\left(\frac{C}{4G}r_{im}^{\alpha-1} + \frac{8\pi}{3Z}a_r^3\right)}{\left(2\sqrt{a_r^2 - 1} + Cr_{im}^{\alpha-1}\right)^3} \tag{24}$$

$$\text{and, } k = \frac{r_{im}^2}{16\left(2\sqrt{a_r^2 - 1} + Cr_{im}^{\alpha-1}\right)\left(D + 2GCr_{im}^{\alpha-1}\right)} \tag{25}$$

The measured porosity, permeability and formation factor of Sample S-28 are 0.297, 5200 md and 9.17, respectively. The optimized parameters are Z = 6, G = 0.042, a_r = 6.705382, C = 1.154587, α = 1.341429, and r_{im} = 19.38799μm. Using these values, the predicted formation factor, porosity and permeability from model simulation are,
ϕ = 0.298, k = 5080md, and F = 9.13, in reasonable agreement with the measured values.

Results and Discussions

Fig.14 shows the resistivity index curves for the three wettability characteristics considered. The interpreted pore size distribution, represented by Fig.6, is utilized with the optimized parameters. The resistivity index for the mixed-wet and oil-wet systems is much higher than that for the water-wet system at low S_w. This indicates that the resistivity of the network is very sensitive to the water in the corners and film. The resistivity index for oil-wet systems is significantly lower than that for water-wet or

mixed-wet systems at high S_w, illustrating the effect of water being redistributed to largest pores in an oil-wet system.

The predicted relative permeability curves to water and oil for three wettability characteristics, obtained using the same set of parameters, are shown in Figs.15 and 16, respectively. Lack of a match indicates that further improvements in the model may be needed. It is observed that there are negligible differences between the water and oil relative permeability curves for the water-wet and mixed-wet systems, indicating that the contribution of the water held in the corners and film may not be quantitatively significant, although it is important for providing hydraulic connectivity. The relative permeability of oil-wet system to water is much larger, whereas to oil is much smaller than for non-oil-wet systems.

Conclusions

Based on the simulation results presented in the preceding, we arrive at the following conclusions:

- The model predictions are most sensitive to the coordination number, followed by shape factor and parameters relating pore throat length to its cross-section.
- Wettability of reservoir rock has a significant effect on the resistivity index and relative permeability curves. Water present in the corners and as film in water-wet systems appears to be very significant to the resistivity index behavior of the reservoir rocks, whereas it appears to have negligible influence on the relative permeability curves.
- A strategy for determining model parameters, based on the measurements of petrophysical properties, capillary pressure curves and wettability of reservoir rocks, has been successfully demonstrated.
- Further improvement are needed in the model for improved prediction of relativepermeability curves

Acknowledgments

We would like to thank the management of Mobil Oil Corporation for their support and for granting the permission to present this paper.

NOMENCLATURE

A = cross section area of sample
A_k = constant in the relationship of film thickness
a_r = aspect ratio
C = constant
$f(r_i)$ = pore size distribution
G = shape factor
$G(g)$ = conductance distribution
g = conductance of pore segment
g_m = conductance of network
h = thickness of thin film
J = curvature
K = absolute permeability
K_r = relative permeability
L_t = length of pore throat
L_b = length of pore body

l_o = constant in the relationship of film thickness
N = sample size
P_c = capillary pressure
P = perimeter of triangle tube
q_w = flow rate of water
q_o = flow rate of oil
R = resistivity
R_t = resistivity of pore throat
R_b = resistivity of pore body
r_b = pore body radius
r_{cd} = drainage radius corresponding to percolation threshold
r_d = drainage radius
r_i = incircle radius
S_w = water saturation
S_{nw} = saturation of non-wetting phase
S = cross section area of triangular tube
V_t = volume of pore throat
V_b = volume of pore body
V_{ps} = volume of pore segment
X_c = percolation threshold
X_a = accessible fraction to non-wetting phase
X_{nw} = allowable fraction to non-wetting phase
Z = coordination number

Greek Symbols

α, β, γ = angles used in the derivation of flow equation
μ_w = viscosity of water
μ_o = viscosity of oil
ρ = resistivity of water
τ = shear stress

Subscript

a = accessible
b = pore body
c = capillary/corner
f = thin film
i = incircle
nw = non-wetting
o = oil
t = pore throat
w = water

REFERENCES

[1] Kirkpatrick, S.: "Percolation and Conduction", Rev. Modern Physics, 45, 574-588 (1973).

[2] Heiba, A. A., Sahimi, M., Scriven, L. E., and Davis, H.T., "Percolation Theory of Two-phase Relative Permeability," SPE Paper 11015, presented at the SPE Annual Meeting, New Orleans, Sept., 1982.

[3] Chatzis, I. and Dullien, F.A.L., "The Modeling of Mercury Porosimetry and the Relative Permeability of Mercury in Sandstones Using Percolation Theory," *Int. Chem. Eng.* 25, 47-66, 1985.

[4] Ehrlich, R. and Davies, D. K., "Image Analysis of Pore Geometry: Relationship to Reservoir Engineering and Modeling," SPE paper 19054, presented at the SPE Gas Technology Symposium, Dallas, TX, June 7-9, 1989.

[5] Wang, J. L., "Simultaneous Prediction of the Electrical Property and Relative Permeability of Reservoir Rocks Using Network Model," Ph. D. Distertation, University of Oklahoma, 1996.

[6] Mason, G. and Morrow, N. R., "Capillary Behavior of a Perfectly Wetting Liquid in Irregular Triangular Tubes," *Journal of Colloid and Interface Science*, Vol. 141, No. 1, January 1991.

[7] Gupta, A. and Sharma, M.M., "Stability of Thin Aqueous Films on Solid Surfaces, II-A Model for Aqueous Films Bounded by Dissimilar Charge Regulating Surfaces," *J. Coll. Int. Sci.*, Vol. 149, No. 2, March 15,1992.

[8] Fisher, M. E. and Essam, J. W., "Some Cluster Size and Percolation Problems," *J. Math. Phys.*, 2, 609-619 (1961).

[9] Larson, R. G., "Percolation in Porous Media with Application to Enhanced Oil Recovery," M.S. Thesis, Chem. Eng., Univ. of Minnesota, Minneapolis (1977).

[10] Larson, R. G. and Morrow, N. R., "Effects of Sample Size on Capillary Pressure in Porous Media," Powder Technol., 30, 123(1981).

[11] Koplik, J., "Creeping Flow in Two-Dimensional Networks," J. Fluid Mech., V. 119, P. 219(1982).

[12] Wang, Y. M., "A Three-Dimensional Network Model for Porous Media," M.S. Thesis, Univ.of Texas at Austin, 1988.

[13] Mishra, B. K. and Sharma, M. M., "Measurement of Pore Size Distributions from Capillary Pressure Curves," *AICHE Journal*, Vol. 34, No .4, April 1988.

[14] Basu, S. and Sharma, M. M., "Investigating the Role of Crude-Oil Components on Wettability Alteration Using Atomic Force Microscopy," SPE paper 37231, presented at the SPE International Symposium on Oilfield Chemistry, Houston, TX, Feb.18-21, 1989.

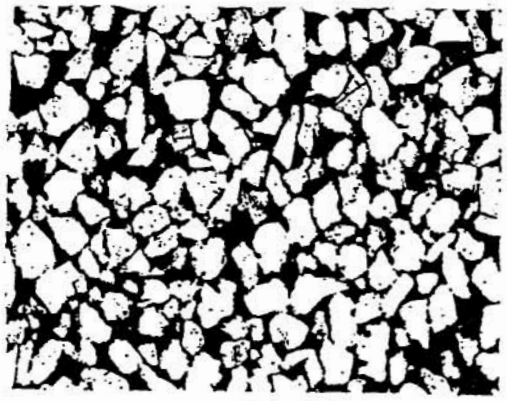

Fig.1 Thin Section Photomicrograph for Sample S-28

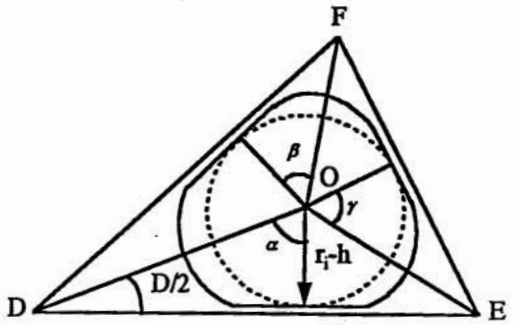

Fig.4 Schematic of Corners and Film in Pore Throat at a Step of Drainage

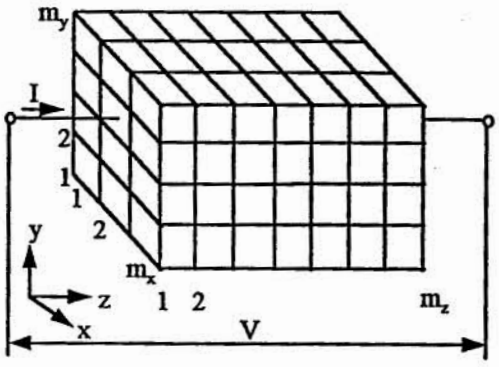

Fig.2 Schematic of the network

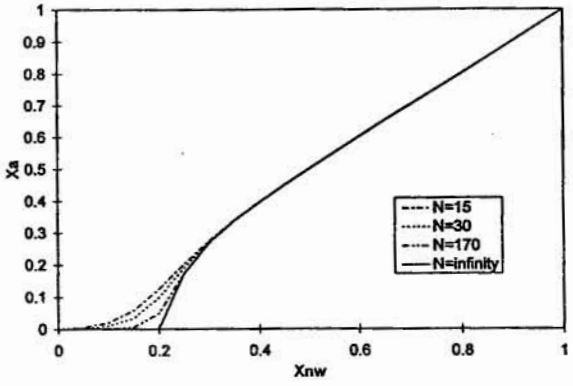

Fig.5 Accessibility Function for Finite and Infinite Lattices(Z = 6)

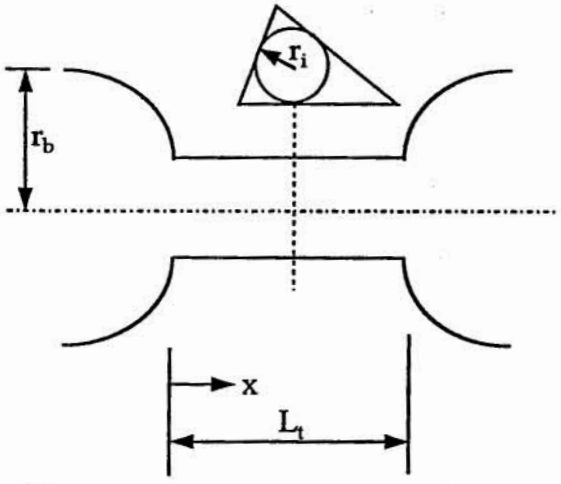

Fig.3 A Pore Segment Schematic

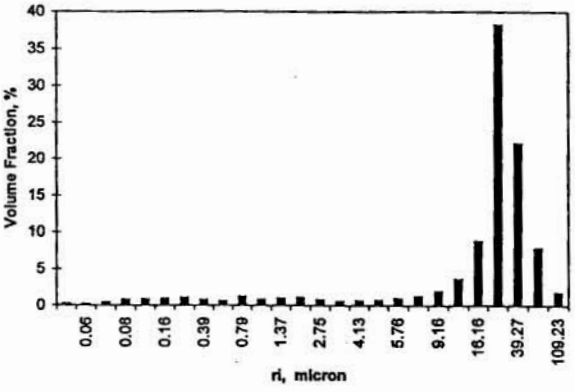

Fig.6 (a) Interpreted Pore Size Distribution (Z = 6, G=0.042)

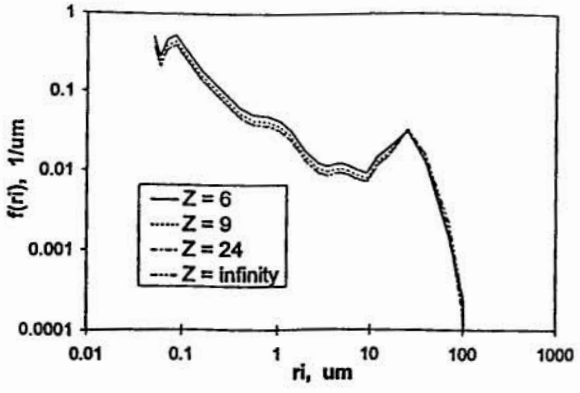

Fig.6 (b) Interpreted Pore Size Distribution for Different Z Values (G=0.04526)

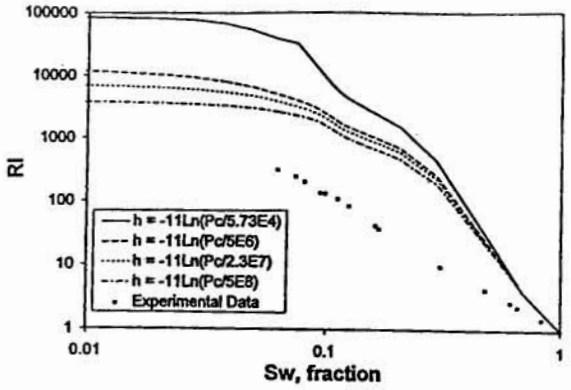

Fig.9 Effect of Film Thickness on Resistivity Index Curve

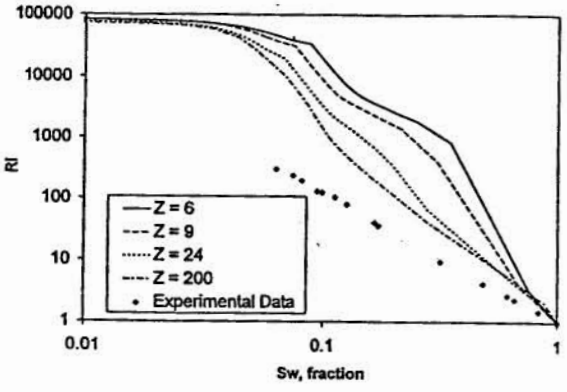

Fig.7 Effect of Coordination Number on Resistivity Index Curve

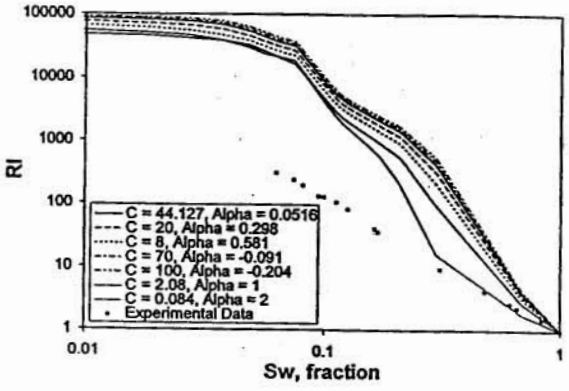

Fig.10 Effect of C and α on Resistivity Index Curve

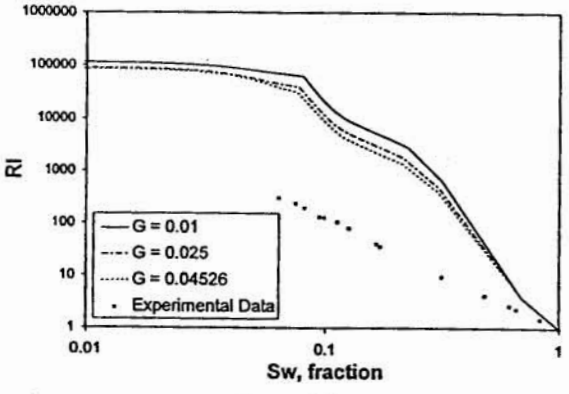

Fig.8 Effect of Shape Factor on Resistivity Index Curve

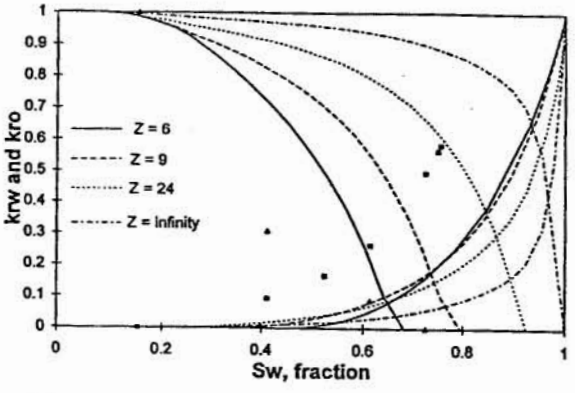

Fig.11 Effect of Coordination Number on Relative Permeability Curves

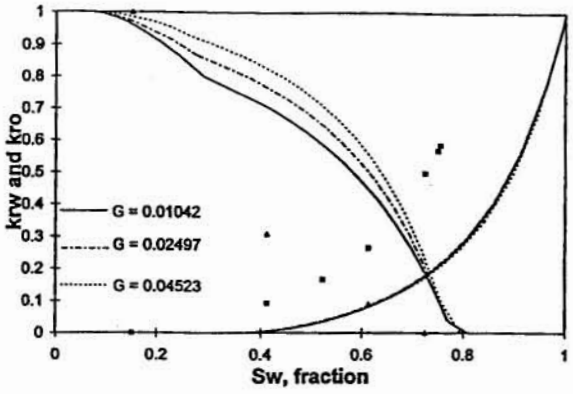

Fig.12 Effect of Shape Factor on Relative Permeability Curves

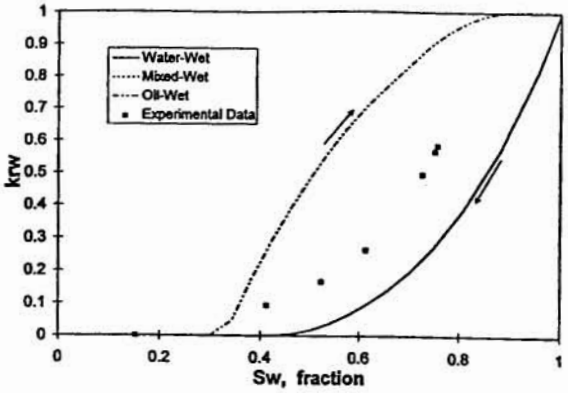

Fig.15 Relative Permeability Curves to Water for Three Wettability Characteristics

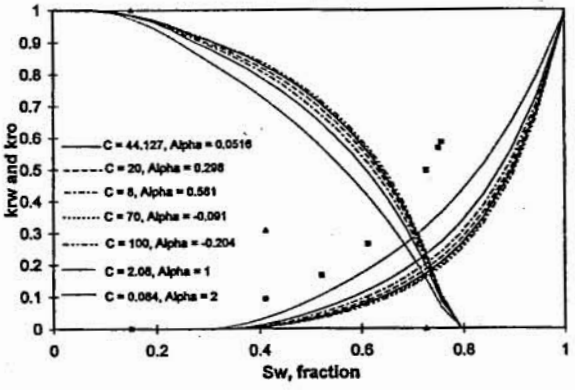

Fig.13 Effect of C and α on Relative Permeability Curves

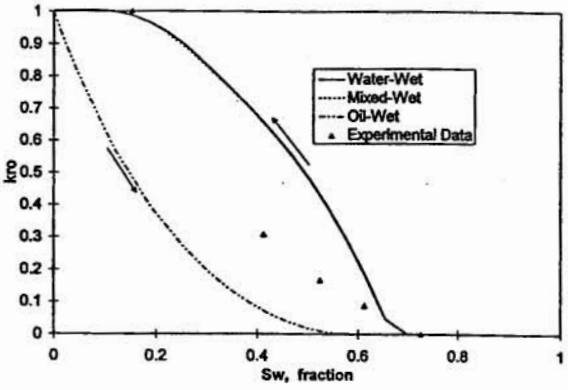

Fig.16 Relative Permeability Curves to Oil for Three Wettability Characteristics

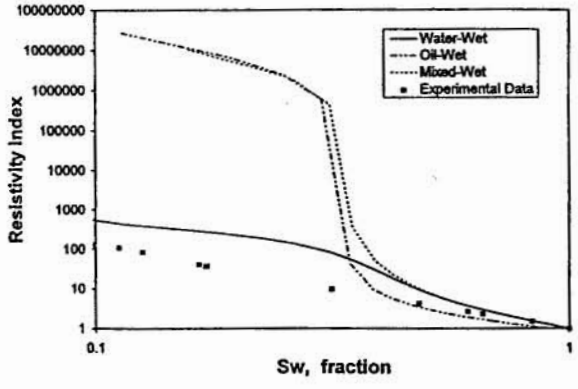

Fig.14 Electrical Resistivity Index Curve for Three Wettability Characteristics